MIMO Channel Rank via the Aperture-Bandwidth Product

Nathan A. Goodman, *Member, IEEE*

***Abstract*— An abstract progressive scattering model for multiple-input, multiple-output (MIMO) wireless communication systems is developed. In the model, the transmitted signal reflects off multiple groups of scatterers on its way from transmit array to receive array. The model is then used to predict the effective degrees of freedom (EDOF) of different stages of propagation within the channel. Using properties of the Karhunen-Loeve expansion of random processes, it is shown that the EDOF of a given stage are controlled by the product of observed spatial bandwidth and observing aperture. Simulated results are then provided to demonstrate how the individual stages interact with each other to determine the EDOF and eigenvalue distribution of the overall MIMO system. These results give additional insight into the behavior of known propagation channels such as keyhole channels and single-bounce channels with receiver-side spatial correlation.**

***Index Terms*— MIMO systems, multipath channels, information rates.**

I. Introduction

MUlti-antenna communication systems [1], [2] have been well investigated in recent years due to their potential for increased spectral efficiency. These multiple-input, multiple-output (MIMO) systems provide large capacity improvements by exploiting multipath rather than combating it. This exploitation takes the form of multiple, spatially parallel communication modes that depend on the eigenvalue distribution of the channel propagation matrix.

The number of parallel communication modes for a MIMO system has sometimes been called the system's effective degrees of freedom (EDOF) [3], [4]. It is well known that spatial correlation at the transmit array, receive array, or both cause a reduction in EDOF with a corresponding decrease in system capacity. Furthermore, it is also known that spatial correlation increases with reduced angular diversity of the incoming multipath. This last fact can be used to explain the poor performance of so-called keyhole channels [5], [6], [7] where limited angle diversity somewhere within the channel itself limits capacity despite favorable correlation properties at both the transmitter and receiver. These general characteristics of MIMO systems are well understood; however, an explicit relationship between physical properties such as the angle-power multipath profile of a communication channel and the EDOF of a MIMO system has not been presented. This paper employs an abstract propagation model that models the propagation between transmitter and receiver as a sequential series of local scattering mechanisms. Each local scattering group observes a given angle-power multipath profile. The Karhunen-Loeve (KL) representation of random processes is then used to characterize and provide intuition about the relationship between the propagation characteristics of individual stages of a MIMO channel and the total system's EDOF.

In work related to this paper, spatial correlation in MIMO channels has been investigated in [3], [4], [5], [6], [8], [9]. In [3], the effects of spatial correlation are studied by varying antenna spacing and multipath angle spread. Moreover, [3] defines the concept of EDOF as being the number of valid parallel communication eigenmodes. Although [3] treats the problem nicely in terms of spatial covariance matrices, quantification of the EDOF based on propagation and antenna array properties is not provided. In [8], it is shown that the asymptotic capacity of correlated fading channels is still linear in the number of antennas, but the slope of the capacity growth is reduced from the uncorrelated case. In [4], asymptotic capacity is investigated while holding the array size fixed. Fixed array size means that antenna separation must decrease as more elements are added, which increases the correlation between adjacent antennas. The results in [4] are obtained using properties of large random matrices.

Correlated fading and keyhole channels are considered in [5], [6], [7]. In [5], examples of outdoor keyhole channels are presented, and a conclusion is made that four-wavelength antenna separation is sufficient given a keyhole channel with scattering over a 30-meter interval (width) that is less than one kilometer away. Requiring the scattering to be within a certain distance ensures a modicum of angular spread that leads to spatial decorrelation with reasonable antenna separation. Very tight upper bounds on mean capacity were provided in [6] for spatially correlated channels with finite transmit and receive antennas. The results in [6] use properties of finite-dimension random matrices rather than the large-matrix properties used in [4]. In [7], a double scattering model is presented and used to demonstrate the existence of keyhole channels that exhibit low channel rank despite uncorrelated spatial fading at the transmit and receive arrays.

Other work characterizes the fundamental MIMO capacity of arrays defined by their length, area, or volume rather than a particular configuration. For example, [10], [11], [12], [13] characterize system capacity as a function of antenna density. In order to remove the SNR advantage obtained by adding more antennas within a fixed volume, [10], [11] apply a total received power constraint rather than the usual constraint on

Manuscript received October 21, 2005; revised June 21, 2006; accepted August 15, 2006. The associate editor coordinating the review of this paper and approving it for publication was M. Shafi.

N. A. Goodman is with the Department of Electrical and Computer Engineering, University of Arizona, 1230 E. Speedway Blvd., Tucson, AZ 85721 (email: goodman@ece.arizona.edu).

Digital Object Identifier 10.1109/TWC.2007.05788.

received power per antenna. In [12], capacity versus antenna density is considered by modeling the multipath environment as a diffusive propagation medium. In [13], specific results are presented for a circular array, but the general conclusion is that capacity increases linearly with the number of antennas until the circular array is well sampled. Beyond this point, additional antennas provide diminished benefit because the MIMO multiplexing gain has already been exploited and maximized.

Generalized capacity results based on fixed antenna array volumes are presented in [14], [15], [16], [17], [18]. In [14], the capacity between a fixed-volume electromagnetic transmitter and a fixed-volume electromagnetic receiver is considered. Since no multipath is modeled, the results in [14] are most applicable to line-of-sight optical communication. In [15], the multipath channel is defined by a Green's function that quantifies the propagation between a fixed transmitting point to a fixed receiving point. The full channel is then determined by integrating the Green's function over the transmitting and receiving volumes. The integration is then approximated with transmit and receive basis functions that can be optimized to find the intrinsic capacity between the two volumes. A similar volume-antenna approach is presented in [16], [17] where it is shown how to calculate the Green's function due specifically to a finite number of scatterers. In [16], [17], capacity is again seen to saturate once the array volumes become well sampled with antennas. Detailed capacity results for single-bounce, clustered-multipath environments is presented in [18]. The results in [18] show that the degrees of freedom due to a single multipath cluster depend on the effective area of the array and the solid angle subtended by the cluster. Other related capacity investigations include a study of capacity versus number of multipath components in [19], capacity in the presence of mutual coupling and antenna loading in [20], and a comparison of experimental and modeled results in [21]. Except where specifically stated, the above investigations focus on single-bounce propagation models.

The areas of MIMO propagation and channel modeling have been treated in [7], [22], [23], [24], [25]. A general overview of antenna and propagation concepts applied to MIMO is provided in [22], including discussions of propagation measurements, modeling approaches, and different channel types. A virtual channel model is described in [23], [24] with the goal of characterizing the relationship between scattering physics and system capacity. Although the virtual model and objective of [23], [24] are similar in spirit to those of this paper, the progressive scattering model and interpretation presented here allow further insight into the behavior of channels such as keyhole channels, which are mentioned but not explicitly treated in [23], [24]. Furthermore, our approach allows us to quantify the number and relative strength of the EDOF as a function of the angular scattering profile. Finally, conditions that produce high-rank versus low-rank MIMO channels are considered in [7] using abstract models for green field (no multipath), single-bounce, and double-bounce channels.

This paper extends the abstract model of [7] to N-bounce scenarios where the transmitted signal reflects off N different groups of scatterers on its way from transmit array to receive array. The scattering from each group is given an average power profile and angle spread that define the power spectral density (PSD) for the spatial random process incident on the next scattering group. In this way, we can use results for the degrees of freedom necessary to represent bandlimited random processes to predict the EDOF of different stages of propagation within the channel. The EDOF of a given stage are controlled by observed spatial bandwidth and observing aperture. Application of these results to the progressive scattering model provides an intuitive demonstration of how the EDOF and propagation paths of different stages interact with each other to determine the EDOF and eigenvalue distribution of the overall system.

The paper is organized as follows. In Section II, we present an abstract, progressive propagation model used in this paper for analysis and simulation. We also investigate properties of the channel model including capacity and overall EDOF. In Section III, we discuss KL representation of random processes, which leads to an aperture-bandwidth product rule for the EDOF of a single propagation stage. Simulated results are shown in Section IV, including results for both single-bounce and double-bounce channels. Some simulations are designed to match single- and double-bounce channels presented elsewhere in the literature, and we show good agreement when this is the case. Furthermore, we can make interesting conclusions about physical channel properties in these situations. Our conclusions are presented in Section V.

II. Propagation Model and Characteristics

In this section, we present the propagation model used in our analysis of multi-antenna wireless systems. The model is capable of representing any spatial correlation structure at the transmitting or receiving array, as well as line-of-sight, single-bounce, keyhole, and progressive-scattering scenarios. Although the model cannot represent the *diagonally correlated* channel investigated in [26], [27], it will be shown that the model can reduce to several special cases considered, for example, in [3], [4], [7], [25].

A. System Model

Consider the situation depicted in Fig. 1 where the signals leaving the n_T antennas of the transmit array successively scatter from N groups of scatterers as they travel from transmit array to receive array. In this process, the signals propagate from the transmit array, then arrive and combine at the first group of scatterers. The signals incident on the first scattering group are then scattered with a random reflection coefficient. The scattered signals then propagate away from the first group toward the second group of scatterers, and so on until the signals are reflected from the last group of scatterers and arrive at the receive array. This type of progressive scattering model has been explored in [28], [29], [30]. In [29], it is argued that propagation between different floors of a building is an example where progressive scattering may be applicable. In [5], it was shown that propagation from a rooftop to a street-level mobile can act as a keyhole channel. Extending this scenario to propagation between multiple rooftops on the way to a mobile is another possible application of the progressive scattering model.

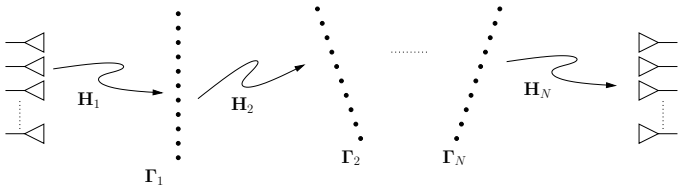

Fig. 1. Progressive scattering model.

The scatterers in each group are effective scatterers that represent the cumulative effects of many physical scatterers located at approximately the same angle of departure or arrival. The effective scatterers represent only the energy that is scattered toward the next scattering group or antenna array, and energy absorbed or scattered in other directions is assumed to be lost. This is similar to the approach taken by many abstract scattering models such as the one-ring model [3], [25], [31] where all physical scattering is represented by a uniformly spaced ring of effective scatterers. Moreover, the one-ring model usually employs known parameters such as the radius of the ring and distance between transmitter and receiver. This leads to deterministic propagation paths between scatterers and antennas, yet the overall channel is still random due to the random scattering coefficient assigned to each effective scatterer. In our model, the relative angles between successive linear arrangements of effective scatterers are known, which leads to deterministic propagation matrices defined below. At each scattering group, however, the scattering coefficients are random, which leads to a random channel as seen by the transmitter and receiver. Each realization of scattering coefficients leads to a different channel realization that must be estimated by the receiver to achieve the available MIMO capacity gain.

Let the n_T-dimensional transmit signal be defined as $\mathbf{x}$. Under the narrowband (frequency flat) assumption, the signal transmitted from the j^{th} antenna arrives at the i^{th} effective scatterer of the first group with complex gain coefficient $\mathbf{H}_1(i,j)$. Hence, the signals incident on the N_1 scatterers of the first group can be described by $\mathbf{y}_1 = \mathbf{H}_1\mathbf{x}$ where $\mathbf{H}_1$ is an $N_1 \times n_T$ matrix of gain coefficients. When we describe scatterers in a group as receiving incident signals, we shall sometimes speak of the scatterers as *nodes* that receive the signals and then scatter the signals toward the next group. We shall also refer to the process of signal propagation between an antenna array and scattering group or between adjacent scattering groups as a single propagation *segment*, or *stage*.

Let the scattering coefficient of the i^{th} scatterer in the first scattering group be $\gamma_{i,1}$ and the $N_1 \times N_1$ scattering matrix for the first group be $\mathbf{\Gamma}_1 = \text{diag}([\gamma_{1,1}\,\gamma_{2,1}\,\cdots\,\gamma_{N_1,1}])$ where $\text{diag}(\cdot)$ denotes the operator that forms a diagonal matrix out of the input array. The N_1-dimensional signal scattered from the first group is $\mathbf{\Gamma}_1\mathbf{H}_1\mathbf{x}$, which then propagates to the next group of scatterers according to propagation matrix $\mathbf{H}_2$. Hence, the signals incident on the second group of scatterers are described by $\mathbf{y}_2 = \mathbf{H}_2\mathbf{\Gamma}_1\mathbf{H}_1\mathbf{x}$. Following this logic, the signal at the n^{th} scattering group is

$$\mathbf{y}_n = \mathbf{H}_n\mathbf{\Gamma}_{n-1}\mathbf{H}_{n-1}\mathbf{\Gamma}_{n-2}\cdots\mathbf{H}_2\mathbf{\Gamma}_1\mathbf{H}_1\mathbf{x} = \tilde{\mathbf{H}}_n\mathbf{x} \quad (1)$$

where

$$\tilde{\mathbf{H}}_n = \mathbf{H}_n\mathbf{\Gamma}_{n-1}\mathbf{H}_{n-1}\mathbf{\Gamma}_{n-2}\cdots\mathbf{H}_1. \quad (2)$$

Finally, the signal at the receive array is

$$\begin{aligned}\mathbf{y}_R &= \mathbf{H}_{N+1}\mathbf{\Gamma}_N\mathbf{H}_N\mathbf{\Gamma}_{N-1}\cdots\mathbf{H}_2\mathbf{\Gamma}_1\mathbf{H}_1\mathbf{x} + \mathbf{n} \\ &= \tilde{\mathbf{H}}_{N+1}\mathbf{x} + \mathbf{n} \end{aligned} \quad (3)$$

where $\mathbf{n}$ is a vector of zero-mean additive white Gaussian noise with independent and identically distributed (i.i.d) circularly symmetric complex Gaussian entries normalized to unit variance. Since the γ's are the scattering coefficients of effective scatterers that represent the contributions of many actual scatterers, it is appropriate to model the γ's as independent and complex Gaussian, which is known as the Rayleigh scattering model [32].

Shortly, we will make the common assumption that a fixed amount of transmit power, P_T, is evenly distributed among the transmit antennas. Under this constraint, the total propagation matrix, $\tilde{\mathbf{H}}_{N+1}$, is usually normalized such that the average SNR at each receiver element is P_T/P_n where $P_n = 1$ is the normalized per-antenna noise power just described. This constraint can be enforced by requiring the reflection coefficients at each scattering stage to satisfy

$$\sum_{i=1}^{N_k} \mathrm{E}[|\gamma_{i,k}|^2] = 1. \quad (4)$$

As seen in Fig. 1, it is assumed that all scatterers within a group lie on a straight line and that the transmit and receive arrays are linear. It is also assumed that the transmit array is in the far field of the first scattering group, that the $(n-1)^{\text{th}}$ scattering group is in the far field of the n^{th} scattering group, and that the N^{th} scattering group is in the far field of the receive array. Nonlinear scatterer and antenna geometries are possible, but the results below depend on the array's effective length, which is more easily demonstrated by beginning with a linear array. Furthermore, the linear scatterer geometry still allows any angular scattering power profile to be implemented. For multipath that spans a large angle spread, the assumption that scatterers or transmit elements lie on a straight line obviously means that the signals from some scattering or transmitting elements must propagate farther than others. The narrowband approximation, however, assumes that the disparity in distance traveled is small compared to the reciprocal of the temporal signal bandwidth. When combined, the far-field and narrowband assumptions force propagation path loss to be nearly constant across all scatterers in a group.

Since the propagation of any one segment of the model is a direct path from one set of nodes to the next, the entries for any given $\mathbf{H}_n$ are deterministic. For example, defining the j^{th} transmit antenna to be at an angle θ_j to the line normal to the first line of scatterers, the above assumptions yield

$$\mathbf{H}_1 = \begin{bmatrix} e^{jk_1 d} & e^{jk_2 d} & \cdots & e^{jk_{n_T} d} \\ e^{jk_1 2d} & e^{jk_2 2d} & & e^{jk_{n_T} 2d} \\ \vdots & & \ddots & \vdots \\ e^{jk_1 N_1 d} & e^{jk_2 N_1 d} & \cdots & e^{jk_{n_T} N_1 d} \end{bmatrix} \quad (5)$$

where d is the spacing between receiving nodes in the first group and $k_j = \frac{2\pi}{\lambda} sin(\theta_j)$ is the spatial frequency of the

plane wave inbound from the j^{th} transmit antenna. Hence, $\mathbf{H}_1$ is the array manifold matrix for a uniform linear array with receive node spacing d. The fact that the entries of $\mathbf{H}_1$ have equal amplitude and can be expressed as phase shifts is a direct consequence of the far-field and narrowband assumptions. The procedure for defining $\mathbf{H}_1$ can be repeated for any $\mathbf{H}_n$ with the $(n-1)^{\text{th}}$ scattering group acting in the role of transmit array.

Each $\mathbf{H}_n$ is deterministic, but in the presence of random scattering, $\mathbf{H}_n\mathbf{\Gamma}_{n-1}$ is random. The diagonal entries of $\mathbf{\Gamma}_{n-1}$ are independent complex Gaussian random variables representing the reflection coefficients of the previous stage's scatterers; hence, the signal received at the n^{th} stage is a linear sum of complex random variables. Furthermore, (5) implies that the j^{th} diagonal entry of $\mathbf{\Gamma}_{n-1}$ is the amplitude of a complex sinusoid with spatial frequency k_j, which means that the signal received at the n^{th} stage is a random process with power spectral density (PSD) defined by the diagonal of $\mathbf{E}[|\mathbf{\Gamma}_{n-1}|^2]$. The absolute bandwidth of the random process is defined by the maximum and minimum k_j, which are determined by the angular spread. The power spectrum of the random process determines the correlation between signals arriving at the receiving nodes.

The fact that the signal at each scattering group is a random process with power spectral density defined by the spread and distribution of scatterers in the previous stage leads to a central theme throughout the rest of this paper. Based on observations concerning the Karhunen-Loeve representation of random processes over a finite interval, we will see that the MIMO EDOF at any stage are determined by the product of spatial frequency spread and receiving aperture. Moreover, the EDOF of the entire system will be less than or equal to the EDOF of any single propagation stage.

B. Model Properties and Examples

We assume that the receiver has perfect channel state information but the transmitter does not. Under these conditions, an appropriate approach is to allocate equal power to each of the transmitting antennas. This leads to

$$I_N = \log_2 \det\left(\mathbf{I}_{n_R} + \frac{P_T}{n_T}\tilde{\mathbf{H}}_{N+1}\tilde{\mathbf{H}}_{N+1}^{\dagger}\right) \tag{6}$$

where I_N is the instantaneous mutual information of an N-stage scattering environment, $\mathbf{I}_n$ is the n-dimensional identity matrix, and P_T is the total power that is divided among all transmit antennas. Since the matrix $\tilde{\mathbf{H}}_{N+1}$ contains random reflection coefficients for $N \geq 1$, the mutual information is random, and we will generally be interested in average mutual information. Consider the $N = 1$ case, which is a single-scattering abstract model [7], [22], [23], [24], [25], [28] shown in Fig. 2. Here, the average mutual information is

$$\mathrm{E}[I_1] = \mathrm{E}\left[\log_2 \det\left(\mathbf{I}_{n_R} + \frac{P_T}{n_T}\mathbf{H}_2\mathbf{\Gamma}_1\mathbf{H}_1\mathbf{H}_1^{\dagger}\mathbf{\Gamma}_1^{\dagger}\mathbf{H}_2^{\dagger}\right)\right]. \tag{7}$$

The matrix $\mathbf{H}_2$ forms linear combinations of the complex Gaussian elements of $\mathbf{\Gamma}_1$, resulting in $\mathbf{H}_2\mathbf{\Gamma}_1$ also having circularly symmetric Gaussian entries. Hence, as in [4], [8], $\mathbf{H}_2\mathbf{\Gamma}_1$ can be factored as $\mathbf{H}_2\mathbf{\Gamma}_1 \overset{\mathfrak{D}}{=} \mathbf{R}_2^{1/2}\mathbf{W}\mathbf{\Psi}^{1/2}$ where $\mathbf{W}$ is a matrix of i.i.d circularly symmetric Gaussian entries with unit variance, $\mathbf{\Psi}^{1/2} = (\mathrm{E}[|\mathbf{\Gamma}_1|^2])^{1/2}$, and the symbol $\overset{\mathfrak{D}}{=}$ means *equally distributed*. This leads to

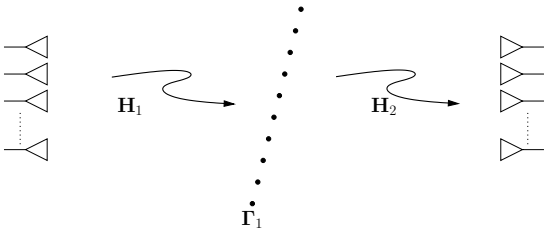

Fig. 2. Single-bounce implementation of the propagation model.

$$\mathrm{E}[I_1] = \mathrm{E}\Big[\log_2 \det\Big(\mathbf{I}_{n_R} + \frac{P_T}{n_T}\mathbf{R}_2^{1/2}\mathbf{W}\mathbf{\Psi}^{1/2}\mathbf{H}_1\mathbf{H}_1^{\dagger}\mathbf{\Psi}^{1/2}\mathbf{W}^{\dagger}\mathbf{R}_2^{1/2}\Big)\Big] \tag{8}$$

where the fact that $\mathbf{R}_2^{1/2} = (\mathbf{R}_2^{1/2})^{\dagger}$ has been exploited. Using the property that $\mathrm{rank}(\mathbf{AB}) \leq \min(\mathrm{rank}(\mathbf{A}), \mathrm{rank}(\mathbf{B}))$, the EDOF of the system are bounded by (note that $\mathrm{rank}(\mathbf{R}_2^{1/2}) = \mathrm{rank}(\mathbf{R}_2)$ and $\mathrm{rank}(\mathbf{R}_1) = \mathrm{rank}(\mathbf{H}_1)$)

$$\mathrm{EDOF} \leq \min(\mathrm{rank}(\mathbf{R}_2), \mathrm{rank}(\mathbf{W}\mathbf{\Psi}^{1/2}), \mathrm{rank}(\mathbf{H}_1)). \tag{9}$$

Therefore, the instantaneous EDOF of the MIMO system are limited by the EDOF of any single propagation stage. In addition, Jensen's inequality allows (8) to be bounded by

$$\begin{aligned}\mathrm{E}[I_1] &\leq \log_2 \det\left(\mathbf{I}_{n_R} + \frac{P_T}{n_T}\mathbf{R}_2^{1/2}\mathrm{E}\Big[\mathbf{W}\mathbf{\Psi}^{1/2}\mathbf{H}_1\mathbf{H}_1^{\dagger}\mathbf{\Psi}^{1/2}\mathbf{W}^{\dagger}\Big]\mathbf{R}_2^{1/2}\right)\\ &= \log_2 \det\Big(\mathbf{I}_{n_R} + \frac{P_T}{n_T}\mathbf{R}_2^{1/2}\mathbf{I}_{n_R}\mathbf{R}_2^{1/2}\Big)\\ &= \log_2 \det\Big(\mathbf{I}_{n_R} + \frac{P_T}{n_T}\mathbf{R}_2\Big).\end{aligned} \tag{10}$$

Hence, average mutual information of the single-bounce model is limited by the eigenvalues of $\mathbf{R}_2$.

Since the signal must propagate through each stage sequentially, application of the data processing theorem [33] states that the mutual information between transmitter and receiver arrays is upper bounded by the mutual information of any single propagation stage. In the single-bounce example above, mutual information is limited by the minimum mutual information supported by either of the two propagation segments, which is to say that

$$I_1 \leq I_0 \tag{11}$$

where I_0 is the mutual information obtained by replacing the single-bounce scattering group with receive antennas. For the general case of N scattering groups and average mutual information, the data-processing argument requires that

$$\mathrm{E}[I_N] \leq \mathrm{E}[I_{N-1}] \leq \cdots I_0. \tag{12}$$

Thus, we observe that the average mutual information of the N-group progressive scattering model is limited not only by the spatial correlation of the final propagation segment, but

also by the spatial correlation of all previous segments. In other words, $\mathrm{E}[I_N]$ is limited by the propagation segment with the worst eigenvalues.

III. Effective Degrees of Freedom and the Aperture-Bandwidth Product

The signal incident on the first scattering group is $\mathbf{y}_1 = \mathbf{H}_1\mathbf{x}$. Noting that the columns of $\mathbf{H}_1$ are complex sinusoids sampled at an interval d, we see that $\mathbf{y}_1$ is a sum of complex sinusoids with random amplitudes. Therefore, the signal incident on the first scattering group is a random process with PSD defined by the average power of the elements of $\mathbf{x}$. For independent Gaussian signaling on each transmit antenna, the random vector $\mathbf{y}_1$ is complex Gaussian due to being a linear combination of $\mathbf{x}$. The covariance matrix of $\mathbf{y}_1$ is

$$\mathrm{E}[\mathbf{y}_1\mathbf{y}_1^\dagger] = \mathbf{H}_1\mathrm{E}[\mathbf{x}_1\mathbf{x}_1^\dagger]\mathbf{H}_1^\dagger = \mathbf{H}_1\left(\frac{P_T}{n_T}\mathbf{I}\right)\mathbf{H}_1^\dagger; \tag{13}$$

hence, we can interpret $\mathbf{y}_1$ as samples of a zero-mean, stationary Gaussian random process with uniform PSD equal to P_T/n_T.

The signal incident on the second scattering group is $\mathbf{y}_2 = \mathbf{H}_2\mathbf{\Gamma}_1\mathbf{H}_1\mathbf{x}$. Again, noting that the columns of $\mathbf{H}_2$ are complex sinusoids sampled at an interval d, we see that $\mathbf{y}_2$ is also a sum of complex sinusoids with random amplitudes. These random amplitudes are the signals scattered from the first set of effective scatterers, which are described by $\mathbf{\Gamma}_1\mathbf{H}_1\mathbf{x} = \mathbf{\Gamma}_1\mathbf{y}_1$. The signal incident on the second scattering group is also a random process, but now the PSD is defined by the average power of the elements of $\mathbf{\Gamma}_1\mathbf{y}_1$. Let the p^{th} entry on the diagonal of $\mathbf{\Gamma}_1$ be $\gamma_{p,1}$ and the p^{th} entry of $\mathbf{y}_1$ be $\mathbf{y}_1(p)$, then the correlation between any two elements of $\mathbf{\Gamma}_1\mathbf{y}_1$ is

$$\begin{aligned}\mathrm{E}[\gamma_{p,1}\mathbf{y}_1(p)\gamma_{q,1}^*\mathbf{y}_1^*(q)] &= \mathrm{E}[\gamma_{p,1}\gamma_{q,1}^*]\mathrm{E}[\mathbf{y}_1(p)\mathbf{y}_1^*(q)] \\ &= \begin{cases}\mathrm{E}[|\gamma_{p,1}|^2]\mathrm{E}[|\mathbf{y}_1(p)|^2], & p = q \\ 0 & p \neq q.\end{cases}\end{aligned} \tag{14}$$

Using (14) and defining a vector of average scattered powers as

$$\begin{aligned}\mathbf{\Psi}_1 = \big[&\mathrm{E}[|\gamma_{1,1}|^2]\mathrm{E}[|\mathbf{y}_1(1)|^2]\ \ \mathrm{E}[|\gamma_{2,1}|^2]\mathrm{E}[|\mathbf{y}_1(2)|^2]\ \ \cdots \\ &\mathrm{E}[|\gamma_{N_s,1}|^2]\mathrm{E}[|\mathbf{y}_1(N_s)|^2]\big]^\dagger\end{aligned} \tag{15}$$

the covariance matrix of $\mathbf{y}_2$ is

$$\begin{aligned}\mathrm{E}[\mathbf{y}_2\mathbf{y}_2^\dagger] &= \mathbf{H}_2\mathrm{E}[\Gamma_1\mathbf{y}_1\mathbf{y}_1^\dagger\Gamma_1^\dagger]\mathbf{H}_2^\dagger \\ &= \mathbf{H}_2\mathrm{diag}(\mathbf{\Psi}_1)\mathbf{H}_2^\dagger.\end{aligned} \tag{16}$$

We can now interpret $\mathbf{y}_2$ as consisting of samples of a zero-mean, stationary random process with PSD equal to the elements of $\mathbf{\Psi}_1$. Each element of $\mathbf{\Psi}_1$ consists of a contribution from the average power incident on the first set of scatterers and a contribution from the scattering coefficient. Since $\mathbf{y}_1$ consists of samples of a stationary random process, the elements of $\mathbf{y}_1$ all have the same average power. Therefore, the shape of the PSD of the random processes observed by the second scattering group is controlled by statistics of the first group's scattering coefficients.

Continuing in this manner, we can show that the signal incident on any scattering group or on the receive array is a random process with PSD defined by the previous group's spread and scattering profile. We now describe how the bandwidth and observation interval of each propagation segment control the EDOF of that segment. We also make general comments concerning the interaction between multiple propagation segments and the EDOF of a progressive-scattering scenario.

The KL expansion represents a random process with a weighted sum of orthonormal functions with uncorrelated coefficients. For example, the orthonormal functions and coefficients for a zero-mean random process are defined by the solutions to

$$\lambda_i\phi_i(x) = \int_0^L K_y(x, x_1)\phi_i(x_1)dx_1 \tag{17}$$

where

$$K_y(x, x_1) = \mathrm{E}[y(x)y(x_1)]. \tag{18}$$

Two interesting properties of the KL expansion can be exploited to estimate the number of non-trivial solutions to (17) and the form of the solutions when the interval L is large [34], [35]. First, when a stationary random process with bandwidth B is observed or represented over a finite aperture L, there are approximately $(BL + 1)$ significant eigenvalues in the KL representation where BL is the aperture-bandwidth product. Second, when the random process is stationary and the observation interval is large, the eigenfunctions become evenly spaced sinusoids whose corresponding eigenvalues are proportional to the process' PSD at that frequency. For the current problem of estimating the EDOF of a MIMO propagation matrix, we saw above that the signal received at the end of each propagation segment is a random process with PSD defined by the previous scattering group's spread and scattering profile. The spatial bandwidth spanned by the random process of a given segment is defined by the span of frequencies seen in the $\mathbf{H}$ matrix for that stage. For example, the spatial bandwidth of the random process $\mathbf{y}_1$ is defined as

$$B_1 = \frac{1}{2\pi}(k_{\max} - k_{\min}) \tag{19}$$

where $k_{\max}$ and $k_{\min}$ are the maximum and minimum spatial frequencies used in the matrix $\mathbf{H}_1$ (see (5)). The spatial aperture of a given stage is defined by the number of receiving nodes and the sample spacing seen in that stage's $\mathbf{H}$ matrix. For example, in (5) the sample interval is d and the number of receiving nodes is N_1, resulting in an aperture of $L_1 = N_1 d$. The first $(B_1L_1 + 1)$ eigenvalues contribute to that segment's capacity while the remaining eigenvalues are too small to make a significant contribution.

While the spatial bandwidth and observation interval of the n^{th} segment determine the EDOF for the n^{th} segment, the second KL property above indicates the values that the eigenvalues will take. Each eigenvalue represents a fraction of the total average power in the random process. The first eigenvalue represents the most powerful region of width Δf possible. The second eigenvalue represents the second-most powerful region of width Δf possible, and so on. Each eigenvalue is proportional to the area under the PSD that it

represents. If the PSD is uniform, then the eigenvalues of the covariance matrix will be uniform. If the PSD is non-uniform, the eigenvalues will follow the non-uniform shape.

We have described the essential physical parameters and processes that determine the EDOF of a MIMO system. The results of Section II describe the relationship between overall system EDOF and the EDOF of individual propagation stages. The results of this section quantify the relationship between EDOF of individual stages and the propagation physics of that stage. In a progressive-scattering scenario, there is interaction between the eigenvalues of the individual propagation segments. A rigorous treatment of this situation requires the theory of products of random matrices and Lyapunov exponents [28], [36]. However, some basic comments can be made. In the following comments, *ordered eigenvalues* refers to ordering instantaneous eigenvalues from largest to smallest. Hence, *the average of the ordered eigenvalues* means that the largest eigenvalues taken from multiple realizations have been averaged, the second-largest eigenvalues have also been averaged, and so on to produce an averaged instantaneous eigenspectrum. The comments are:

- For the $N = 0$ case, there is no multiple-stage interaction and no random scattering, and the average of the ordered eigenvalues of the system are identical to the eigenvalues of the receive correlation matrix, leading to instantaneous capacity that equals mean capacity.
- For $N \geq 1$, (9) shows that the EDOF of the system will be equal to the minimum of the EDOF of any single propagation segment. The non-zero eigenvalues tend to become more non-uniform as more stages are added.
- For $N \geq 1$, if any given stage has an aperture-bandwidth product much less than the aperture-bandwidth products of all other stages, the average of the ordered eigenvalues of the system tend to follow the eigenvalues of that stage. Consequently, average mutual information will approach the mutual information of that stage. This is particularly important for keyhole channels ($N \geq 2$ with rank of at least one segment ≈ 1).
- For $N = 1$, if the transmit-to-scatterer segment exhibits zero correlation, the average of the ordered eigenvalues of the system will approach the eigenvalues of the receive covariance matrix. This conclusion is a specific case of the previous property. Furthermore, as the number of scatterers in the scattering group becomes large, the instantaneous eigenvalues of the system approach the eigenvalues of the receive covariance matrix almost surely (as seen in [4]).

IV. Results

In this section, we set up the abstract progressive scattering model to represent various propagation channels found in the literature. In the following, all spatial frequencies are normalized to wavelength spacing. Thus, if a spatial frequency is $f_s = \frac{1}{\lambda}\sin\theta$, the normalized spatial frequency is $\lambda f_s = \sin\theta$. If a receive array observes multipath arrivals over the full range of angles from $-\pi/2$ to $\pi/2$ (due to the symmetry of a linear array, additional angles need not be considered), this convention leads to a normalized spatial frequency bandwidth equal to two.

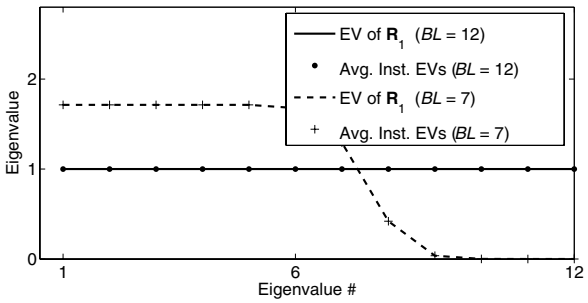

Fig. 3. Covariance matrix eigenvalues vs. instantaneous eigenvalues for a green-field scenario with variable spacing between receive antennas.

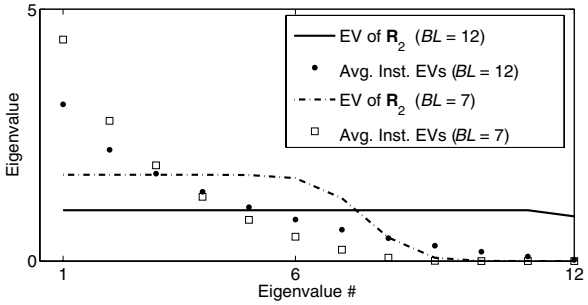

Fig. 4. Covariance matrix eigenvalues vs. averaged instantaneous eigenvalues for a single-bounce scenario with equal aperture-bandwidth products on the transmit and receive segments.

First, consider the $N = 0$ case where no multipath propagation exists. With no multipath propagation, the instantaneous mutual information of the system is equal to the average mutual information because there are no mechanisms in the propagation physics that cause randomness. In Fig. 3 we see that the eigenvalues (EV) begin to sharply decrease at the point where the eigenvalue number approaches the product of system array aperture and spatial bandwidth, BL. The simulation used to produce Fig. 3 used 12 transmitting and 12 receiving antennas, and the receive antenna spacing for the two curves was 0.5 and 0.3 wavelengths. The aperture-bandwidth product for the two cases was 12 and seven as indicated in the plot. In these results, a uniform power spectral density was applied, which explains why the eigenvalues are nearly flat until dropping off around the EDOF predicted by the aperture-bandwidth product. The properties of the KL representation being exploited here are asymptotic properties that become valid at large aperture-bandwidth product. If many more antennas were available and aperture-bandwidth product was increased, the drop-off in eigenvalues would be sharper. For practical antenna arrays, however, the drop-off is smoothed. The peak eigenvalue level decreases with increasing aperture-bandwidth product due to the constant receiver power collected by a fixed number of receive antennas. Therefore, when the EDOF decrease, the same total received power is concentrated within fewer eigenvalues.

A single-bounce scenario is shown in Fig. 4. The number of transmit and receive antennas was 12 while the number of effective scatterers was 100. The separation between scattering nodes in the first propagation stage was equal to 0.06 and

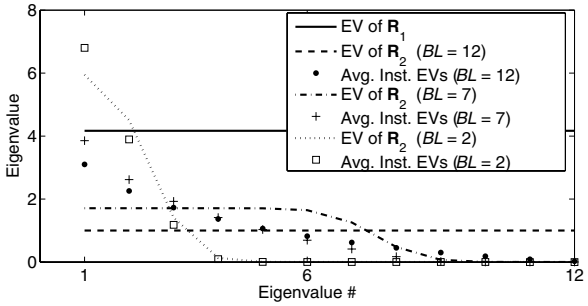

Fig. 5. Covariance matrix eigenvalues vs. averaged instantaneous eigenvalues for a single-bounce scenario with unequal aperture-bandwidth products on the transmit and receive segments.

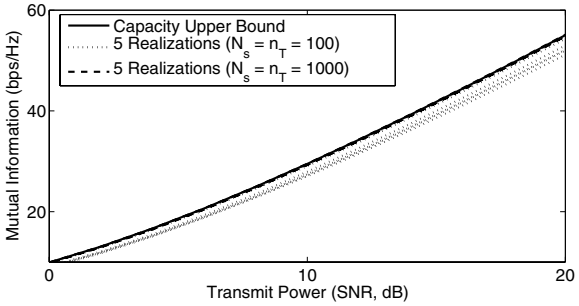

Fig. 6. Capacity of random channel realizations versus number of scatterers, $\mathbf{N_s}$, making up the channel and the number of transmit antennas.

0.035 wavelengths for the two cases shown and the receive array antenna spacing was 0.5 and 0.3 wavelengths. These spacings led to identical aperture-bandwidth products at the two propagation stages. These products are seen in Fig. 4 to be 12 and seven. Figure 4 shows the eigenvalues of the receive covariance matrix. The eigenvalues of the covariance matrix at the scattering nodes (not shown) have the same shape, but are larger because 100 scattering nodes collect more total energy than the 12 receive antennas. The averaged eigenvalue curve is obtained by ordering the eigenvalues from largest to smallest for each channel realization. The largest eigenvalues of each realization are then averaged together, the second largest are averaged together, and so on.

Due to the KL properties described earlier, the eigenvalues of the covariance matrix are relatively flat in accordance with the flat PSD of the propagation processes. It is interesting to see that the number of nonzero instantaneous eigenvalues is strictly limited to less than the number of nonzero eigenvalues of the covariance matrices. However, the instantaneous eigenvalues are not identical to the covariance eigenvalues as they were in Fig. 3. This is due to the random scattering present in the single-bounce model. Since the reflection coefficients are random, each realization of the random channel has a particular path or paths that are dominant despite the uniform scattering profile that makes all paths equal on average. The largest instantaneous eigenvalue will always represent the dominant path, leading to non-uniform instantaneous eigenvalues.

A single-bounce scenario is also investigated in Fig. 5, but in this case the angle spreads of the two propagation segments are allowed to differ. The receive array spacing was held constant at 0.5 wavelengths. The spatial bandwidth observed by the first scattering group due to signals arriving from the transmit array was assumed to be the full bandwidth of two for all cases. In the first case, the aperture-bandwidth products of the two segments are both 12. The eigenvalues of the covariance matrix for the first segment are higher than those of the receive segment because there are more scattering nodes than receive antennas. Hence, although the average incident power is unity for both segments, the scatterers in the first segment collect more total energy than the 12 receivers in the receive segment. As the spatial bandwidth of the second (receive) propagation segment is reduced, the aperture-bandwidth product of the second segment reduces to seven and two. It is clear that the number of nonzero instantaneous eigenvalues is limited by the segment with the worst correlation properties. These results indicate that the EDOF of the overall system is approximately equal to the minimum aperture-bandwidth product of any of the propagation stages.

In [4], a case was shown where the instantaneous capacity converged almost surely to the mean capacity for the case of spatial correlation at the receive array but perfectly uncorrelated transmit elements. If this were the case in Fig. 5, we would see instantaneous eigenvalues equal to the covariance eigenvalues as in Fig. 3. The result in [4] was obtained using asymptotic properties of large random matrices, which in our model implies a large number of scatterers and transmit elements. Consider the situation where the aperture-bandwidth product of the transmit side is much larger than the aperture-bandwidth product on the receive side. This implies that the receiver correlation is the limiting factor in capacity. Next, assume that the number of scatterers, and therefore the number of unique propagation paths, is approximately equal to the receiver-side aperture bandwidth product. In this case, the number of propagation paths is approximately the same as the EDOF. Since each scatterer has a random reflection coefficient, there will always be dominant paths, leading to instantaneous eigenvalues that don't conform to the spatial PSD that governs the propagation. In other words, the instantaneous spatial spectrum does not equal the expected spatial spectrum. As the number of scatterers increases, however, the situation changes. All of the scattered power must be represented in the eigenvalues of the propagation matrix. Therefore, as the number of scatterers increases beyond the EDOF of the system, each eigenvalue must represent the contributions of more than one scatterer. As the number of scatterers becomes large, each eigenvalue must represent the contributions of many propagation paths. When many propagation paths contribute to a single eigenmode, the individual fluctuations of paths will be smoothed. This leads to instantaneous eigenvalues that approach the eigenvalues of the covariance matrix.

The effect of increasing the number of scatterers and transmitters for fixed receive-side aperture-bandwidth product is shown in Fig. 6. In Fig. 6, the number of scattering and transmit elements was varied from 100 to 1000 (the number of transmitters must increase with the number of scatterers to prevent spatial correlation on the transmit side). The receive-side aperture-bandwidth product was six. The aperture-bandwidth

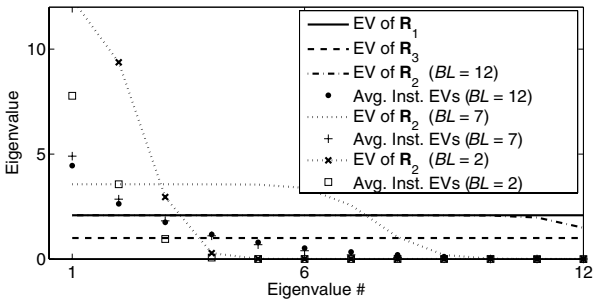

Fig. 7. Covariance matrix eigenvalues vs. averaged instantaneous eigenvalues for a double-bounce scenario with varying aperture-bandwidth product in the second propagation segment. As this product becomes small, the channel becomes a keyhole channel with limited MIMO gain.

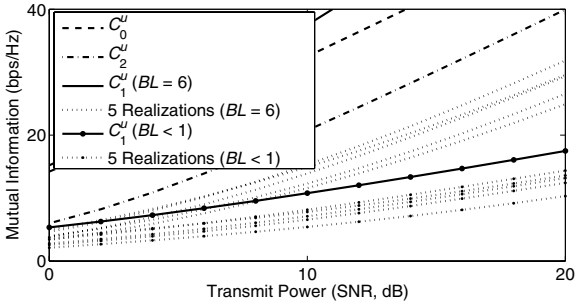

Fig. 8. Capacity bounds and instantaneous capacity as the aperture-bandwidth product of the middle stage of a double-bounce scenario is reduced. For small aperture-bandwidth product, the channel becomes a so-called keyhole channel.

product of the first propagation segment was equal to the number of scatterers, N_s. For each case, capacity is evaluated over five realizations of the channel. The solid line shows the upper bound on average mutual information obtained through Jensen's inequality using the eigenvalues of the receive covariance matrix. Since the receiver-side correlation function is fixed, the bound curve is identical for both cases. For 100 scatterers, it is seen that the mean of the realizations approaches the capacity bound, which is a result of the overall system being limited by the receiver-side propagation. As the number of scatterers increases, however, the random realizations become less variable and more tightly follow the upper bound. For 1000 scatterers, the random realizations are in agreement with the almost-sure convergence described in [4]. In fact, for this case the random realization curves are barely distinguishable due to their being within the line thickness of the bound curve.

Based on this analysis, we can gain additional insight into the result presented in [4]. At first, the result is counterintuitive in that many different channels could be realized that conform to the channel's correlation properties. For example, it is statistically possible for only a single scatterer to have a non-zero reflection coefficient. This would only leave one propagation path, which clearly does not provide the richness needed for MIMO gain. We can now see, however, that the large-matrix approximation implies a large number of scatterers, and as the number of scatterers increases, the smoothing effect described above occurs. In other words, the correlation function defines the required multipath angle spread and spatial power profile. The large-matrix approximation requires that the channel be rich not only in angle spread, but also in the number of scatterers, which makes it increasingly unlikely for the channel to be as atypical as in the example above.

Finally, we consider a propagation scenario with two scattering groups in Figs. 7 and 8. In Fig. 7, the number of scatterers in each group is 25 while there are 12 transmit and 12 receive antennas. The spacing between scatterers is 0.24 wavelengths and the spacing between receive antennas is 0.5 wavelengths. The aperture-bandwidth products for the first and third stages are both equal to 12, which implies rich scattering and wide angle spread. In the first case, the aperture-bandwidth product for the second stage is also 12, which leads to many nonzero instantaneous eigenvalues with uneven average distribution. In the second case, the normalized spatial bandwidth of the second stage is decreased to 1.2, which decreases the aperture-bandwidth product to seven. The number of nonzero instantaneous eigenvalues is approximately seven in this case despite the rich scattering around the transmitter and receiver. Finally, the aperture-bandwidth product is further reduced to approximately two with the corresponding decrease in nonzero instantaneous eigenvalues.

As the aperture-bandwidth product of the second propagation stage in Fig. 7 is reduced from 12 to two, the number of parallel communication modes decreases proportionately. For smaller aperture-bandwidth product, this double-bounce model becomes a keyhole channel [5], [6], [7], [22], which is well known to have poor MIMO gain despite favorable correlation properties at the transmit and receive arrays. The instantaneous rank of the overall propagation matrix is limited by the minimum aperture-bandwidth product of any propagation stage, which gives further intuition about the performance of channels such as keyhole channels. The effect on mutual information of changing the aperture-bandwidth product of the second propagation stage is presented in Fig. 8. We have also reduced the number of transmit and receive antennas to 6 to further demonstrate that our conclusions are applicable to more realistic antenna arrays. In Fig. 8, we show upper bounds on capacity determined by the eigenvalues of the spatial covariance matrix for each of the three propagation segments. As the angle spread of the second segment is reduced, so do the corresponding bound C_1^u and instantaneous capacity curves. When the second stage's aperture-bandwidth product is much less than the other stages, it becomes the bottleneck in the system, which is now a keyhole channel. The upper bound of the second segment also becomes tighter as the disparity between the capacity of the middle segment and the other segments increases.

V. Conclusions

While it has been understood for some time that spatial correlation limits the EDOF of a multi-antenna communication system, the relationship between the channel physics and EDOF have not been fully explored. Furthermore, the poor capacity properties of keyhole channels have been observed and modeled, but intuition about how the physics of the keyhole channel relates to EDOF and capacity has been lacking. In this paper, we have presented an abstract progressive

scattering model and an aperture-bandwidth product technique that can be used to explore these relationships for many types of channels. The model is validated by comparing results for channels modeled elsewhere in the literature.

Using properties of the KL representation of random processes, we related the EDOF produced by multipath propagation to the product of spatial frequency bandwidth and observing interval. Then, using the progressive scattering model and simple relationships for the rank of products of matrices, we demonstrated that the instantaneous EDOF of a multi-antenna system are limited by the minimum aperture-bandwidth product of any single propagation segment. Furthermore, when the aperture-bandwidth product of a single stage is much less than the aperture-bandwidth product of all other stages, mean capacity is bounded by the capacity of that stage. As the disparity between aperture-bandwidth products becomes larger, the bound becomes tighter. These properties provide physical intuition about the known behavior of channels such as keyhole channels and single-bounce channels without transmitter-side spatial correlation.

REFERENCES

[1] I. Teletar, "Capacity of multi-antenna gaussian channels," *European Trans. Telecommun.*, vol. 10, no. 6, pp. 586–595, 1999.

[2] G. Foschini and M. Gans, "On limits of wireless communication in a fading environment when using multiple antennas," *Wireless Personal Commun.*, vol. 6, no. 3, pp. 311–335, 1998.

[3] D. Shiu, G. Foschini, M. Gans, and J. Kahn, "Fading correlation and its effect on the capacity of multielement antenna systems," *IEEE Trans. Commun.*, vol. 48, no. 3, pp. 502–513, 2000.

[4] S. Wei, D. Goeckel, , and R. Janaswamy, "On the asymptotic capacity of MIMO systems with antenna arrays of fixed length," *IEEE Trans. Wireless Commun.*, vol. 4, no. 4, pp. 1608–1621, 2005.

[5] D. Chizhik, G. Foschini, M. Gans, and R. Valenzuela, "Keyholes, correlations, and capacities of multielement transmit and receive antennas," *IEEE Trans. Wireless Commun.*, vol. 1, no. 2, pp. 361–368, 2002.

[6] H. Shin and J. Lee, "Capacity of multiple-antenna fading channels: spatial fading correlation, double scattering, and keyhole," *IEEE Trans. Inf. Theory*, vol. 49, no. 10, pp. 2636–2647, 2003.

[7] D. Gesbert, H. Bolcskei, D. Gore, and A. Paulraj, "Outdoor MIMO wireless channels: models and performance prediction," *IEEE Trans. Commun.*, vol. 50, no. 12, pp. 1926–1934, Dec. 2002.

[8] C. Chuah, D. Tse, J. Kahn, and R. Valenzuela, "Capacity scaling in MIMO wireless systems under correlated fading," *IEEE Trans. Inf. Theory*, vol. 48, no. 3, pp. 637–650, 2002.

[9] S. Loyka and A. Kouki, "On the use of jensen's inequality for MIMO channel capacity estimation," in *Proc. Canadian Conference on Electrical and Computer Engineering*, vol. 1, May 2001, pp. 475–480.

[10] D. Gesbert, T. Ekman, and N. Christophersen, "Capacity limits of dense palm-sized MIMO arrays," in *Proc. IEEE Global Comm. Conf. (Globecom)*, vol. 2, 2002, pp. 1187–1191.

[11] N. Chiurtu, B. Rimoldi, and E. Telatar, "Dense multiple antenna systems," in *Proc. IEEE Inf. Theory Workshop*, 2001, pp. 108–109.

[12] A. Moustakas, *et al*., "Communication through a diffusive medium: coherence and capacity," *Science*, vol. 287, pp. 287–290, 2000.

[13] T. Pollock, T. Abhayapala, and R. Kennedy, "Antenna saturation effects on MIMO capacity," in *Proc. IEEE International Conf. on Comm.*, May 2003, pp. 2301–2305.

[14] D. Miller, "Communicating with waves between volumes: evaluating orthogonal spatial channels and limits on coupling strengths," *Applied Optics*, vol. 39, no. 11, pp. 1681–1699, 2000.

[15] J. Wallace and M. Jensen, "Intrinsic capacity of the MIMO wireless channel," in *Proc. IEEE International Ant. and Prop. Symp.*, 2002, pp. 696–700.

[16] L. Hanlen and M. Fu, "Wireless communications systems with spatial diversity: a volumetric model," *IEEE Trans. Wireless Commun.*, vol. 5, no. 1, pp. 133–142, 2006.

[17] ——, "Capacity of MIMO channels: a volumetric approach," in *Proc. IEEE International Conf. on Comm.*, May 2003, pp. 3001–3005.

[18] A. Poon, R. Brodersen, and D. Tse, "Degrees of freedom in multiple-antenna channels: a signal space approach," *IEEE Trans. Inf. Theory*, vol. 51, no. 2, pp. 523–536, 2005.

[19] V. Raghavan and A. Sayeed, "MIMO capacity scaling and saturation in correlated environments," in *Proc. IEEE International Conf. on Comm.*, May 2003, pp. 3006–3010.

[20] J. Wallace and M. Jensen, "The capacity of MIMO wireless systems with mutual coupling," in *Proc. IEEE Vehicular Tech. Conf.*, Fall 2002, pp. 696–700.

[21] ——, "Statistical characteristics of measured MIMO wireless channel data and comparison to conventional models," in *Proc. IEEE Vehicular Tech. Conf.*, Fall 2001, pp. 1078–1082.

[22] M. Jensen and J. Wallace, "A review of antennas and propagation for MIMO wireless communications," *IEEE Trans. Antennas Propag.*, vol. 52, no. 11, pp. 2810–2824, 2004.

[23] A. Sayeed, "Deconstructing multiantenna fading channels," *IEEE Trans. Signal Processing*, vol. 50, no. 10, pp. 2563–2579, 2002.

[24] A. Sayeed and V. Veeravalli, "Essential degrees of freedom in time and frequency selective MIMO channels," *Wireless Personal Multimedia Commun.*, vol. 1, pp. 107–111, 2002.

[25] R. Ertel, et al., "Overview of spatial channel models for antenna array communication systems," *IEEE Personal Commun.*, vol. 5, no. 1, pp. 10–22, 1998.

[26] H. Ozcelik, N. Czink, and E. Bonek, "What makes a good MIMO channel model?" in *Proc. IEEE Veh. Tech. Conf.*, Spring 2005, pp. 156–160.

[27] H. Ozcelik, et al., "Deficiencies of 'kronecker' MIMO radio channel model," *Electron. Lett.*, vol. 39, no. 16, pp. 1209–1210, 2003.

[28] A. Tulino and S. Verdu, *Random Matrix Theory and Wireless Communications*. Hanover, MA: Now Publishers, 2004.

[29] R. Muller, "On the asymptotic eigenvalue distribution of concatenated vector-valued fading channels," *IEEE Trans. Inf. Theory*, vol. 48, no. 7, pp. 2086–2091, 2002.

[30] S. Saunders, *Antennas and Propagation for Wireless Communication Systems*. Chichester, UK: Wiley, 1999.

[31] W. Jakes, *Microwave Mobile Communications*. New York: John Wiley and Sons, 1974.

[32] N. Levanon, *Radar Principles*. New York: Wiley, 1988.

[33] R. Fano, *Transmission of Information: A Statistical Theory of Communications*. New York: MIT Press, 1961.

[34] H. Landau and H. Pollak, "Prolate spheroidal wave functions, fourier analysis and uncertainty - iii: The dimension of the space of essentially time- and band-limited signals," *Bell Syst. Tech. J.*, vol. 41, pp. 1295–1336, 1962.

[35] H. L. V. Trees, *Detection, Estimation, and Modulation Theory, Part I*. New York: John Wiley and Sons, 1968.

[36] H. Furstenberg and H. Kesten, "Products of random matrices," *Annals of Math. Statistics*, pp. 457–469, 1960.

Nathan A. Goodman (S'98-M'02) received the B.S., M.S., and Ph.D. degrees in electrical engineering from the University of Kansas, Lawrence, in 1995, 1997, and 2002, respectively.

From 1996 to 1998, he was an RF Systems Engineer for Texas Instruments, Dallas, TX. From 1998 to 2002, he was a Graduate Research Assistant in the Radar Systems and Remote Sensing Laboratory, University of Kansas. He is currently an Assistant Professor in the Department of Electrical and Computer Engineering, University of Arizona, Tucson. Within the department, he directs the Laboratory for Sensor and Array Processing. His research interests are in radar and array signal processing.

Dr. Goodman was awarded the Madison A. and Lila Self Graduate Fellowship from the University of Kansas in 1998. He was also awarded the IEEE 2001 International Geoscience and Remote Sensing Symposium Interactive Session Prize Paper Award.